Compensating Network Dynamics in Grid-Forming Control

Dominic Groß

***Abstract*—The circuit dynamics of power networks are typically neglected in transient stability analysis of power systems. While this approximation is justified in classical multi-machine power systems, the circuit dynamics can compromise stability of power systems dominated by grid-forming (GFM) power converters. In this work, we show that the impact of circuit dynamics can be mitigated by (i) augmenting GFM droop control with derivative feedback, and (ii) leveraging derivative control terms of dual-port GFM control that was recently proposed in the literature. Moreover, we show that, contrary to conventional wisdom, avoiding instability by slowing down the converter dynamics (e.g., through virtual inertia) is not always possible or may require unrealistic virtual inertia constants.**

I. Introduction

Tomorrow's electric power systems are envisioned to be sustainable, resilient, and largely based on renewable generation and power electronics. Replacing conventional fuel-based synchronous generators with converter-interfaced resources results in significantly different power system dynamics and challenges standard power system models, analysis methods, and operating paradigms [1]. For instance, compared to synchronous machines power electronic converters have limited inherent energy storage and overload capability. On the other hand, compared to the relatively slow physics of a synchronous machines, the dynamic response of power electronic converter are mainly prescribed by fast and flexible control.

Broadly speaking, control strategies for grid-connected dc/ac voltage source converters (VSC) are typically categorized into (i) grid-forming (GFM) strategies that impose a well-defined ac voltage waveform (e.g., frequency and magnitude) at the point of connection, and (ii) grid-following (GFL) controls that can only operate if another device (e.g., synchronous generator) imposes a near nominal ac voltage waveform (e.g., frequency and magnitude) at their point of interconnection. In particular, GFL control is fragile under weak grid coupling [2] and may fail due to voltage disturbances [3] or in systems without sufficiently tight frequency control.

In contrast, power converters with GFM control are envisioned to be the cornerstone of future power systems [1], [4], [5]. The prevalent approaches to GFM control are droop control [6], [7], virtual synchronous machine control [8], virtual oscillator control [9], [10], and dispatchable virtual oscillator control [11]. While the need for emulating synchronous machines and their inertia has always been the subject of debate [1], [4], recent results indicate that leveraging the fast frequency response capabilities of grid-forming converters offers advantages over emulating the relatively slow synchronous machine dynamics [12]–[14].

At the same time, it has been observed that the network circuit dynamics can compromise the stability of microgrids [15], [16] and converter-dominated power systems [11], [17]. This instability cannot be detected using quasi-steady-state network models widely used in system-level stability analysis [11], [15]–[17] and is commonly attributed to a lack of timescale separation between the converter controls and network dynamics [17]. In other words, according to conventional wisdom, multimachine systems do not exhibit this phenomenon because the machine voltage phase angles change slowly relative to the settling time of the network circuit dynamics.

On the other hand, analytical stability conditions for droop control and a reduced-order dynamic microgrid model [18] and dispatchable virtual oscillator control and a dynamic π-line model [11], [19] reveal low inductance, large droop gains, and low resistance-reactance ratios as the main salient features of power systems that exhibit instability due to interactions between GFM controls and network circuit dynamics [11], [18], [19]. However, the aforementioned works do not investigate compensating the network dynamics by slowing down the GFM controls (e.g., inertia emulation) or similar means.

Conceptually, [15]–[17] aim to develop models that can be used to detect instabilities induced by network circuit dynamics. However, detailed network models may not scale to large systems and detailed network data may not be available for bulk systems. More importantly, while scalable high-fidelity network modeling is interesting in its own right, this approach does not improve the stability boundary related to network circuit dynamics but merely quantifies it. Instead, this work aims to compensate the destabilizing effect of network circuit dynamics through device-level control and thereby justify the use of low-complexity quasi-steady-state network models for the vast majority of system-level analysis tasks.

To this end, this work first develops a small-signal model that accounts for the dynamics of resistive-inductive networks with homogenous converter controls and uniform resistance-reactance ratio. Using this model, we first obtain analytic stability conditions for droop control and virtual synchronous machine control. The results show that slowing down the converter voltage phase angle dynamics through inertia emulation to increasing the timescale separation between the network and converter dynamics may not be effective. Specifically, contrary to conventional wisdom, increasing the timescale separation through inertia emulation cannot always stabilize the overall system or may require unrealistic virtual inertia constants. Next, we investigate compensating the network circuit dynamics by (i) augmenting droop control with a

This material is based upon work supported by the U.S. Department of Energy's Office of Energy Efficiency and Renewable Energy (EERE) under the Solar Energy Technologies Office Award Number 38637 and DE-EE0009024. The views expressed herein do not necessarily represent the views of the U.S. Department of Energy or the United States Government.

D. Groß is with the Department of Electrical and Computer Engineering at the University of Wisconsin-Madison, USA; e-mail: dominic.gross@wisc.edu

realizable derivative droop [20], and (ii) leveraging a derivative droop term inherent in dual-port GFM control [21], [22]. This approach significantly improves the stability boundary for droop control with small low pass filter time constants and dual-port GFM control of voltage source converters with small internal energy storage. Finally, we propose and analyze a combined frequency and angle droop control that leverages proportional angle droop to improve the stability boundary for arbitrary droop gains and virtual inertia constants.

Notation

Given an angle $\theta \in \mathbb{R}$ we define the rotation

$$\mathbf{R}(\theta) \coloneqq \begin{bmatrix} \cos(\theta) & -\sin(\theta) \\ \sin(\theta) & \cos(\theta) \end{bmatrix}, \quad \mathbf{r}(\theta) \coloneqq \begin{bmatrix} \cos(\theta) \\ \sin(\theta) \end{bmatrix},$$

and the $90°$ rotation matrix $j \coloneqq \mathbf{R}(\pi/2)$ that can be interpreted as an embedding of the complex imaginary unit $\sqrt{-1}$ into $\mathbb{R}^2$. Given a matrix A, A^T denotes its transpose. For column vectors $x \in \mathbb{R}^n$ and $y \in \mathbb{R}^m$ we use $(x, y) = [x^\mathsf{T}, y^\mathsf{T}]^\mathsf{T} \in \mathbb{R}^{n+m}$ to denote a stacked vector. Moreover, I_n, $\mathbb{0}_{n\times m}$, and $\mathbb{1}_{n\times m}$ denote the $n \times n$ identity matrix and $n \times m$ matrices of zeros and ones. The cardinality of a set $\mathcal{X} \subset \mathbb{N}$ is denoted by $|\mathcal{X}|$.

II. Power System model

A. Network topology

We study the control of three-phase voltage source converters (VSCs) interconnected through a power network modeled by resistive-inductive lines. All electrical quantities in the network are assumed to be balanced. Each VSC imposes an ac voltage at a bus of the power network. The power network is modeled as a connected simple[1] graph $\mathcal{G} = (\mathcal{N}, \mathcal{E}, \mathcal{W})$, where $\mathcal{N}$ is the set of nodes (i.e., buses) corresponding to the voltage source converters, $\mathcal{E} \subseteq (\mathcal{N} \times \mathcal{N}) \setminus \cup_{i\in\mathcal{N}}(i, i)$, with $|\mathcal{E}|$, is the set of edges corresponding to the transmission lines, and $\mathcal{W}$ is a set of edge weights corresponding to the inverse line inductance. The topology of the power network is modeled by the oriented incidence matrix $B \in \{-1, 0, 1\}^{|\mathcal{N}|\times|\mathcal{E}|}$.

B. Network dynamics

The dynamics of the current across a transmission line connecting the nodes $(n, k) \in \mathcal{E}$ are modeled by

$$\ell_{nk} \tfrac{\mathrm{d}}{\mathrm{d}t} i_{nk} = -(r_{nk} I_2 + j\omega_0 \ell_{nk}) i_{nk} + v_n - v_k, \qquad (1)$$

where $i_{nk} = (i_{d,nk}, i_{q,nk}) \in \mathbb{R}^2$, $v_n \in \mathbb{R}^2$, and $v_k \in \mathbb{R}^2$ denote the current across the line $(n, k) \in \mathcal{E}$, voltage at the bus $l \in \mathcal{N}$, and voltage at bus $k \in \mathcal{N}$ in a dq-frame rotating at the nominal frequency $\omega_0 \in \mathbb{R}_{>0}$. Moreover, $\ell_{nk} \in \mathbb{R}_{>0}$ and $r_{nk} \in \mathbb{R}_{>0}$ denote the line inductance and resistance. To simplify the analysis, we assume that the resistance-reactance ratio is identical throughout the network. This assumption is typically justified for lines at the same voltage level.

[1] In other words, undirected and containing no self-loops or multiple edges.

Assumption 1 (Uniform resistance-inductance ratio) *The resistance-inductance ratio $\rho_{\frac{r}{l}} = \frac{r_{nk}}{\ell_{nk}}$ and resistance-reactance ratio $\rho_{\frac{r}{x}} = \frac{r_{nk}}{\omega_0 \ell_{nk}}$ are identical for all $(n, k) \in \mathcal{E}$.*

Moreover, we require the following definition of instantaneous three-phase power.

Definition 1 (Branch power and bus power injection) *Given the bus voltage $v_n \in \mathbb{R}^2$, we define the branch power $p_{nk} \coloneqq v_n^\mathsf{T} i_{nk}$ and bus power injection $p_n \coloneqq \sum_{k:(n,k)\in\mathcal{E}} p_{nk} \in \mathbb{R}$.*

The bus voltages are modeled in polar coordinates $v_n \coloneqq V_n \mathbf{r}(\theta_n)$ with phase angle $\theta_n \in \mathbb{R}$ and magnitude $V_n \in \mathbb{R}$. Selecting the phase angle differences $\theta_{nk} = \theta_n - \theta_k$ as input, and linearizing $p_{nk} = v_n^\mathsf{T} i_{nk}$ and (1) at $\theta_n = \theta_k$ and $V_n = V_k = V^\star$ results in

$$p_{nk}(s) = \frac{1}{\ell_{nk}} \underbrace{\frac{\omega_0 V^{\star 2}}{s^2 + 2\rho_{\frac{r}{l}} s + \omega_0^2 + \rho_{\frac{r}{l}}^2}}_{=: g_{p,\theta}(s)} \theta_{nk}(s). \qquad (2)$$

Considering Assumption 1 and Definition 1, the small-signal dynamics of the overall power network are given by

$$p(s) = BW g_{p,\theta}(s) B^\mathsf{T} \theta(s) = g_{p,\theta}(s) L \theta(s), \qquad (3)$$

where $p \coloneqq (p_1, \ldots, p_{|\mathcal{N}|}) \in \mathbb{R}^{|\mathcal{N}|}$ and $\theta \coloneqq (\theta_1, \ldots, \theta_{|\mathcal{N}|}) \in \mathbb{R}^{|\mathcal{N}|}$ are the bus power injections and voltage phase angles, $W \coloneqq \operatorname{diag}\{\ell_{n_e k_e}^{-1}\}_{e=1}^{|\mathcal{E}|} \in \mathbb{R}^{|\mathcal{E}|\times|\mathcal{E}|}$ collects the inverse line inductance, and $L \coloneqq BWB^\mathsf{T} \in \mathbb{R}^{|\mathcal{N}|\times|\mathcal{N}|}$ is the Laplacian matrix associated with the graph $\mathcal{G}$.

C. Voltage source converter dynamics

Each three-phase VSC imposes an ac voltage with and phase angle $\theta_n \in \mathbb{R}$ (relative to a frame rotating at the nominal frequency ω_0) and magnitude $V_n \in \mathbb{R}$ at its point of connection. For small-signal frequency stability analysis, the ac voltage magnitude is typically assumed to be nominal [23, Sec. 6]. Moreover, the VSC dynamics of each VSC are modeled by a transfer function $g_{\mathrm{vsc},n}(s)$ from its power injection p_n to its frequency ω_n. To simplify the analysis, we assume that the dynamics of each VSC are identical up to scaling by the VSC rating. This assumption is often made in the analysis of multi-machine and multi-converter systems and, amongst other properties, ensures load sharing in proportion to the rating of each converter.

Assumption 2 (Homogeneous and stable control) *Consider a transfer function $g_{\omega,p}(s)$ that has all its zeroes and poles in the open left half plane and relative degree greater than or equal to minus one. Given the converter rating $\gamma_n \in \mathbb{R}_{>0}$, $g_{\mathrm{vsc},n}(s) = \gamma_n^{-1} g_{\omega,p}(s)$ holds for all $n \in \mathcal{N}$.*

Based on this assumption, the VSC model is given by

$$\theta_n(s) = -\frac{1}{s} g_{\omega,p}(s) \frac{1}{\gamma_n} \big(p_n(s) + \delta_{p,n}(s)\big) + \delta_{\theta,n}(s), \qquad (4)$$

where $\delta_{p,n} \in \mathbb{R}$ denotes a load perturbation at the converter buses. Moreover, $\delta_{\theta,n} \in \mathbb{R}$ denotes a constant disturbance

input accounting for the fact that the VSCs local angle references are not identical (i.e., VSCs not have access to a common clock or angle reference). Notably, $g_{\omega,p}(s)$ need not be realizable, because grid-forming control of VSCs only requires θ_l. Hence it suffices that $\frac{1}{s}g_{\omega,p}(s)$ is realizable.

D. Power system frequency dynamics

Defining $\omega := (\omega_1, \dots, \omega_{|\mathcal{N}|}) \in \mathbb{R}^{|\mathcal{N}|}$, $\delta_p := (\delta_{p,1}, \dots, \delta_{p,|\mathcal{N}|}) \in \mathbb{R}^{|\mathcal{N}|}$, $\delta_\theta := (\delta_{\theta,1}, \dots, \delta_{\theta,|\mathcal{N}|}) \in \mathbb{R}^{|\mathcal{N}|}$, and $\Gamma := \operatorname{diag}\{\gamma_n\}_{n=1}^{|\mathcal{N}|} \in \mathbb{R}^{|\mathcal{N}|\times|\mathcal{N}|}$, the overall power system frequency dynamics shown in Fig. 1 are obtained.

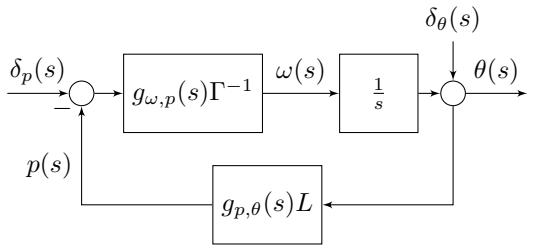

Fig. 1. Power system dynamics with load perturbations δ_p, reference angle offsets δ_θ, converter frequency ω, and voltage phase angle θ.

III. Preliminary results

A. Diagonalization and stability

To simplify the analysis, we apply the same ideas as in [24] to diagonalize the power system dynamics. Rescaling by the matrix of converter ratings Γ and rearranging the block diagram results in the equivalent power system dynamics shown in Fig. 2. Moreover, we define the scaled Laplacian matrix $L_\Gamma := \Gamma^{-\frac{1}{2}} L \Gamma^{-\frac{1}{2}} \in \mathbb{R}^{N\times N}$ and $N := |\mathcal{N}|$. Notably, L_Γ can be decomposed into $L_\Gamma = M\Lambda M^\mathsf{T}$ with an orthonormal matrix $M \in \mathbb{R}^{N\times N}$ and diagonal matrix $\Lambda = \operatorname{diag}\{\lambda_n\}_{n=1}^N \in \mathbb{R}^{N\times N}$ of eigenvalues $\lambda_1 = 0 \le \lambda_2 \le \dots \le \lambda_N$ of L_Γ. Rescaling the power system dynamics by M results in the equivalent diagonalized power system dynamics shown in Fig. 3. Considering that $MM^\mathsf{T} = I_N$ and $g_{\omega,p}$ is stable by Assumption 2, it directly follows that stability of the overall power system is equivalent to stability of

$$g_\lambda(s) := \frac{g_{\omega,p}(s)}{1 + \frac{\lambda}{s} g_{\omega,p}(s) g_{p,\theta}(s)} \tag{5}$$

for all $\lambda \in \{\lambda_2, \dots, \lambda_N\}$. Moreover, because $g_{\omega,p}$ is stable and minimum-phase, stability of $g_\lambda(s)$ for all $\lambda \in \{\lambda_2, \dots, \lambda_N\}$ is equivalent to stability of $g_{\lambda_N}(s)$ (i.e., $g_\lambda(s)$ with $\lambda = \lambda_N$).

B. Synchronization

Next, we note that the transfer function from the reference angle offset δ_0 to the voltage phase angle θ is given by

$$g_{\theta,\delta_\theta}(s) := \Gamma^{-\frac{1}{2}} M \operatorname{diag}\left\{g_{\omega,p}(s)^{-1} g_\lambda(s)\right\}_{\lambda=0}^{\lambda_N} M^\mathsf{T} \Gamma^{\frac{1}{2}}. \tag{6}$$

By Assumption 2, $g_{\omega,p}(s)^{-1}$ is asymptotically stable. Thus, stability of $g_{\lambda_N}(s)$ implies stability of $g_{\theta,\delta_\theta}(s)$ and $g_{\omega,\delta_\theta}(s) := s g_{\theta,\delta_\theta}(s)$. The next result shows that constant angle offsets

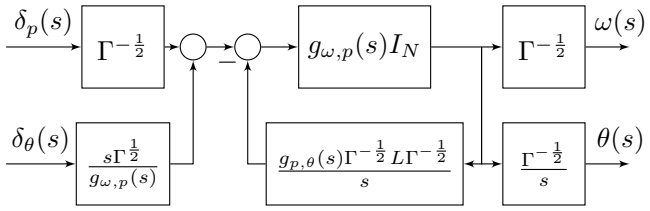

Fig. 2. Power system dynamics after rescaling by the converter rating Γ and moving the disturbance input δ_θ.

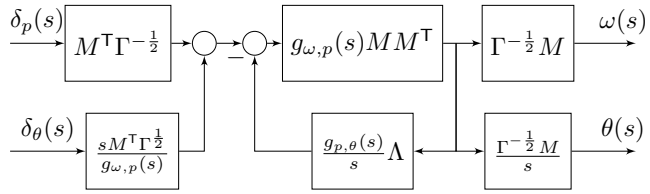

Fig. 3. Closed-loop power system dynamics after diagonalization of the scaled Laplacian matrix L_Γ.

$\delta_\theta \in \mathbb{R}^N$ do not affect the steady-state frequency and that the phase angles $\theta \in \mathbb{R}^N$ synchronize for any constant $\delta_\theta \in \mathbb{R}^N$. While this property is well established for standard grid-forming controls that correspond to realizable transfer functions $g_{\omega,p}$, it needs to be revisited for the broader class of controls considered in Assumption 2.

Lemma 1 (Frequency stability and angle synchronization) *Consider a controller $g_{\omega,p}$ such that Assumption 2 holds. It holds that $\lim_{s\to 0} g_{\omega,\delta_\theta}(s) = \mathbb{0}_{N\times N}$. Moreover, for any $\delta_0 \in \mathbb{R}^N$, it holds that $\lim_{s\to 0} g_{\theta,\delta_\theta}(s)\delta_0 = \operatorname{span} \mathbb{1}_N$.*

Proof: Consider a generic controller $g_{\omega,p} = \frac{b_{d+1}s^{d+1}+\dots+b_0}{a_d s^d+\dots+a_0}$. It can be verified that

$$\lim_{s\to 0} \frac{g_\lambda(s)}{g_{\omega,p}(s)} = \lim_{s\to 0} \frac{1}{1 + \frac{\lambda}{s} g_{\omega,p}(s) g_{p,\theta}(s)} = \lim_{s\to 0} \frac{1}{\frac{\lambda}{s}\frac{b_0}{a_0}\frac{\omega_0 V^{\star 2}}{\omega_0^2 + \rho_T^2}}.$$

Moreover, Assumption 2 implies that $b_0/a_0 \in \mathbb{R}_{>0}$ and it follows that $\lim_{s\to 0} g_{\omega,p}(s)^{-1} g_\lambda(s) = 0$ for all $\lambda > 0$ and $\lim_{s\to 0} g_{\omega,p}(s)^{-1} g_\lambda(s) = 1$ if $\lambda = 0$. Next, using $M = [M_1, \dots, M_N]$ it follows that $\lim_{s\to 0} g_{\theta,\delta_\theta}(s) = \Gamma^{-\frac{1}{2}} M_1 M_1^\mathsf{T} \Gamma^{\frac{1}{2}}$. Moreover, $M_1 = (\sum_{n\in\mathcal{N}} \gamma_n)^{-\frac{1}{2}} \Gamma^{\frac{1}{2}} \mathbb{1}_n$ (see e.g., [24]) and $\lim_{s\to 0} g_{\theta,\delta_\theta}(s) = (\sum_{n\in\mathcal{N}} \gamma_n)^{-1} \mathbb{1}_{N\times N} \Gamma$. Finally, using the same arguments, it follows that $\lim_{s\to 0} g_{\omega,\delta_\theta}(s) = \lim_{s\to 0} s g_{\theta,\delta_\theta}(s) = \mathbb{0}_{N\times N}$. ■

C. Spectrum of the scaled Laplacian L_Γ

Using quasi-steady-state network models commonly considered in the literature[2] and leveraging standard arguments (see e.g., [24]), the fact that $\frac{\lambda}{s}$ is positive real guarantees stability for any λ_N and any strictly positive real converter control $g_{\omega,p}(s)$. However, the dynamic network model (3) results in the diagonalized network model $\frac{\lambda}{s} g_{p,\theta}(s)$ that cannot

[2]In other words, using $g_{p,\theta}(s) = \frac{V^{\star 2}\omega_0 \ell_0^2}{\omega_0^2 \ell_0^2 + r_0^2}$.

be positive real because the relative degree of $g_{p,\theta}(s)$ exceeds one [25]. Broadly speaking, λ_N can be interpreted as the maximum gain of the VSC's interactions through the network and significantly impacts stability.

To clarify how λ_N scales with the network inductances ℓ_{nk} and converter ratings γ_n, we define the weighted node degree $d_n := \sum_{k:(n,k)\in\mathcal{E}} \frac{1}{\gamma_n \ell_{nk}}$ and maximum local ratio of ratings $\sigma_n := \max_{k:(n,k)\in\mathcal{E}} \frac{\gamma_n}{\gamma_k}$.

Lemma 2 (Laplacian spectrum) *The largest eigenvalue λ_N of the scaled Laplacian L_Γ is bounded by*

$$\max_{n\in\mathcal{N}} d_n \leq \lambda_N \leq \max_{n\in\mathcal{N}} (1+\sqrt{\sigma_n})\, d_n.$$

Proof: By construction of L_Γ it holds for all $n \in \mathcal{N}$ that $(L_\Gamma)_{n,n} = \sum_{k:(n,k)\in\mathcal{E}} \gamma_n^{-1}\ell_{nk}^{-1}$. Moreover, for all $n \neq k$, it holds that $(L_\Gamma)_{n,k} = -\gamma_n^{-\frac{1}{2}}\gamma_k^{-\frac{1}{2}}\ell_{nk}^{-1}$. Noting that $\gamma_k \geq \frac{1}{\sigma_n}\gamma_n$ and applying Gershgorin's circle theorem results in

$$\lambda_N \leq \max_{n\in\mathcal{N}} \sum_{k:(n,k)\in\mathcal{E}} \frac{1}{\gamma_n \ell_{nk}} + \sum_{k:(n,k)\in\mathcal{E}} \frac{1}{\sqrt{\gamma_k\gamma_n}\ell_{nk}}, \tag{7a}$$

$$\lambda_N \leq \max_{n\in\mathcal{N}} \sum_{k:(n,k)\in\mathcal{E}} \frac{1}{\gamma_n \ell_{nk}} + \sqrt{\sigma_n} \sum_{k:(n,k)\in\mathcal{E}} \frac{1}{\gamma_n \ell_{nk}}. \tag{7b}$$

Moreover, using the Rayleigh quotient it follows that

$$\lambda_N = \max_{\|\chi\|=1} \chi^\mathsf{T} L_\Gamma \chi \leq \sum\nolimits_{k:(n,k)\in\mathcal{E}} \gamma_n^{-1}\ell_{nk}^{-1}. \tag{8}$$

The lemma direct follows by definition of d_n. ∎

In other words, the upper and lower bound on λ_N increase as the rating of the converter with maximum weighted node degree $d_{\max} := \max_{n\in\mathcal{N}} d_n$ decreases. Moreover, the upper bound on λ_N increases if the maximum ratio $\sigma_{\max} := \max_{n\in\mathcal{N}} \sigma_n$ of ratings increases (i.e., if neighboring converters have significantly different ratings). Finally, both the upper and lower bound on λ_N scale with the inverse inductance, i.e., decreasing the inductance between the converter with maximum weighted node degree and its neighbors increases $d_{\max}$ and λ_N.

IV. Stability conditions without compensation of network circuit dynamics

We will first investigate stability of $g_{\lambda_N}(s)$ for standard droop control and virtual synchronous machine control without compensation of network circuit dynamics.

A. Droop control and virtual synchronous machines

The most prevalent grid-forming control is so-called droop control [6], [7]. Droop control is based on the assumption that the internal dynamics of the VSC can be neglected. In this case, the VSC frequency is given by the controller

$$g_{\text{dr}}(s) = \frac{m_p}{Ts+1}. \tag{9}$$

In other words, letting $g_{\omega,p}(s) = g_{\text{pd}}(s)$, the VSC model (4) becomes

$$\theta_n(s) = -\left(\frac{1}{s}\frac{m_p}{Ts+1}\right)\frac{p_n(s)+\delta_{p,n}(s)}{\gamma_n} + \delta_{\theta,n}(s).$$

Moreover, changing coordinates, virtual synchronous machine (VSM) control [8] with virtual inertia $M \in \mathbb{R}_{>0}$ and virtual damping $D \in \mathbb{R}_{>0}$ in proportion to the VSM rating is equivalent to (9) with $m_p = 1/D$ and $T = M/D$ (see [26]).

Remark 1 (Frequency droop gain) *In the context of power systems, the droop gain m_p is typically prescribed by system operators, aggregators, markets, or grid codes to meet system-level control objectives. Therefore, it is not a degree of freedom that can be tuned to ensure stability of the system.*

The next result provides sufficient conditions for stability of the overall power system with converters using droop control or virtual synchronous machine control.

Theorem 1 (Stability of droop control) *Consider $g_{\omega,p}(s) = g_{\text{dr}}(s)$. Then, $g_{\lambda_N}(s)$ is asymptotically stable if one of the following holds*

(i) $T = 0$ and for all $n \in \mathcal{N}$ it holds that

$$(1+\sqrt{\sigma_n})d_n m_p V^{\star 2} < 2\omega_0^2\left(\rho_{\frac{r}{x}} + \rho_{\frac{r}{x}}^3\right),$$

(ii) $T \geq 0$, $\rho_{\frac{r}{x}} < 1$, and for all $n \in \mathcal{N}$ it holds that

$$(1+\sqrt{\sigma_n})d_n m_p V^{\star 2} < \omega_0^2\left(\rho_{\frac{r}{x}} + \rho_{\frac{r}{x}}^3\right).$$

Proof: For $T = 0$ the Hurwitz criterion $g_{\lambda_N}(s)$ guarantees asymptotic stability of $g_{\lambda_N}(s)$ if and only if $2\rho_{\frac{r}{l}} \in \mathbb{R}_{>0}$, $\lambda_N m_p V^{\star 2}\omega_0 \in \mathbb{R}_{>0}$, $\omega_0^2 + \rho_{\frac{r}{l}}^2 + \lambda_N m_p V^{\star 2}\omega_0 \in \mathbb{R}_{>0}$, and $2\rho_{\frac{r}{l}}(\omega_0^2 + \rho_{\frac{r}{l}}^2) > \lambda_N m_p V^{\star 2}\omega_0$. Then, the first statement directly follows from Lemma 2. Moreover, $g_{\lambda_N}(s)$ is asymptotically stable for $T \in \mathbb{R}_{>0}$ if and only if $2T\rho_{\frac{r}{l}} + 1 > 0$, $\lambda m_p V^{\star 2}\omega_0 \in \mathbb{R}_{>0}$, and

$$\begin{aligned} 4\rho_{\frac{r}{l}}^2\left(\frac{1}{2}\rho_{\frac{r}{l}}^{-1}(\omega_0^2+\rho_{\frac{r}{l}}^2)^2 - \lambda_N m_p V^{\star 2}\omega_0\right)T^2 + \\ 4\rho_{\frac{r}{l}}\left(\rho_{\frac{r}{l}}(\omega_0^2+\rho_{\frac{r}{l}}^2) - \lambda_N m_p V^{\star 2}\omega_0\right)T + \\ 2\rho_{\frac{r}{l}}(\omega_0^2+\rho_{\frac{r}{l}}^2) - \lambda_N m_p V^{\star 2}\omega_0 > 0. \end{aligned} \tag{10}$$

Next, if $\frac{\omega_0\ell_0}{r_0} > 1$ and $\frac{r_0}{\omega_0}(\omega_0^2+\rho_{\frac{r}{l}}^2) > m_p(1+\sqrt{\sigma_n})d_n V^{\star 2}$, it follows that $\frac{1}{2}\rho_{\frac{r}{l}}^{-1}(\omega_0^2+\rho_{\frac{r}{l}}^2)^2 > 2\rho_{\frac{r}{l}}(\omega_0^2+\rho_{\frac{r}{l}}^2) > \rho_{\frac{r}{l}}(\omega_0^2 + \rho_{\frac{r}{l}}^2) > \lambda_N m_p\omega_0 V^{\star 2}$, i.e., (10) holds for any $T \in \mathbb{R}_{>0}$ and the second statement follows from Lemma 2. ∎

Loosely speaking the stability conditions for droop control without low-pass filter (i.e., $T = 0$) highlight that increasing the droop gain m_p, increasing the voltage magnitude $V^\star$, decreasing the resistance-inductance ratio $\rho_{\frac{r}{l}}$, and increasing d_n or σ_n for the converter $n \in \mathcal{N}$ with maximum $(1+\sqrt{\sigma_n})d_n$ will result in instability. Moreover, we recall that d_n increases as the line length and converter rating decrease, and $\sqrt{\sigma_n}$ increases as the difference between converter ratings increases.

The second statement highlights that stability is ensured for all $T \in \mathbb{R}_{\geq 0}$ if the resistance-reactance ratio $\rho_{\frac{r}{x}}$ is small enough and $(1+\sqrt{\sigma_n})d_n$ is small enough for all converters $n \in \mathcal{N}$. This is typically the case in high-voltage transmission systems with resistance-reactance ratio $\rho_{\frac{r}{x}} \ll 1$, long transmission lines, and transformers that add

significant impedance to the lines, i.e., approximately result in relatively large values of ℓ_{nk} and small values for d_n. However, considering Lemma 2, the results also highlight that d_n may significantly increase and result in instability in future transmission systems that may contain many devices with low rating connected through short lines (i.e., within a wind farm).

Remark 2 (Decentralized & centralized stability conditions) *The stability conditions developed throughout this work can be verified in a decentralized fashion if every converter $n \in \mathcal{N}$ has access to ℓ_{nk} and γ_k for all k with $(n,k) \in \mathcal{E}$. On the other hand, if the network data is available to a centralized coordinator it suffices to check the stability conditions for the converter $n \in \mathcal{N}$ with maximum $(1+\sigma_n)d_n$.*

Conventional wisdom suggests that inertia emulation may be used to slow down the dynamics of the phase angle $\theta \in \mathbb{R}^n$ relative to the network dynamics (3) and thereby enforce the timescale separation of classical multi-machine systems. However, the next result shows that this is may not be the case. In particular, if droop control with no inertia emulation is not stable (i.e., the conditions for $T = 0$ do not hold) and the resistance-reactance ratio $\rho_{\frac{r}{x}}$ is large, then no amount of virtual inertia will stabilize the system.

Theorem 2 (Instability of droop control) *Consider $g_{\omega,p}(s) = g_{\text{dr}}(s)$. Then, $g_{\lambda_N}(s)$ is not asymptotically stable if there exists $n \in \mathcal{N}$ such that*

$$m_p d_n V^{\star 2} > 2\omega_0^2 \left(\rho_{\frac{r}{x}} + \rho_{\frac{r}{x}}^3\right)$$

and either (i) $T = 0$ or (ii) $T \geq 0$ and $\rho_{\frac{r}{x}} > \sqrt{\frac{1}{3}}$.

Proof: Following the same arguments as in the proof of Theorem 1, asymptotic stability of $g_{\lambda_N}(s)$ with $T = 0$ requires $\rho_{\frac{r}{l}}(\omega_0^2 + \rho_{\frac{r}{l}}^2) > \frac{1}{2}\lambda_N m_p V^{\star 2}\omega_0$. However, by Lemma 2 it holds that $\max_{n\in\mathcal{N}} d_n \leq \lambda_N$ and, under the hypothesis of this Theorem, it holds that $\rho_{\frac{r}{l}}(\omega_0^2 + \rho_{\frac{r}{l}}^2) < \frac{1}{2}\lambda_N m_p V^{\star 2}\omega_0$. Moreover, if $\rho_{\frac{r}{x}}^{-1} < \sqrt{3}$ and $\rho_{\frac{r}{x}}(\omega_0^2 + \rho_{\frac{r}{l}}^2) < \frac{1}{2} m_p d_n V^{\star 2}$ for any $n \in \mathcal{N}$, then $\frac{1}{2}\rho_{\frac{r}{x}}^{-1}(\omega_0^2 + \rho_{\frac{r}{l}}^2)^2 < 2\rho_{\frac{r}{l}}(\omega_0^2 + \rho_{\frac{r}{l}}^2) < d_n m_p V^{\star 2}\frac{\omega_0}{\ell_0} < \lambda_N m_p V^{\star 2}\omega_0$. This also implies that $\rho_{\frac{r}{l}}(\omega_0^2 + \rho_{\frac{r}{l}}^2) < \lambda_N m_p V^{\star 2}\omega_0$ and (10) cannot hold for any $T \geq 0$. ■

The previous two results cover two limit cases of systems with droop controlled converters that are stable for any time constant $T \geq 0$ (Theorem 1.ii) or unstable for any time constant $T \geq 0$ (Theorem 2.ii). The corresponding regions in the parameter space for a system of two converters with equal rating are illustrated in Fig. 5.

The next result provides a necessary condition that illustrates that the filter time constant $T \geq 0$ (i.e., virtual inertia constant) required to stabilize the system in the remaining cases may be excessive. In particular, large time constants $T \geq 0$ are problematic from a practical point of view because they can typically only be realized by a VSC with significant energy storage and peak power capabilities [5].

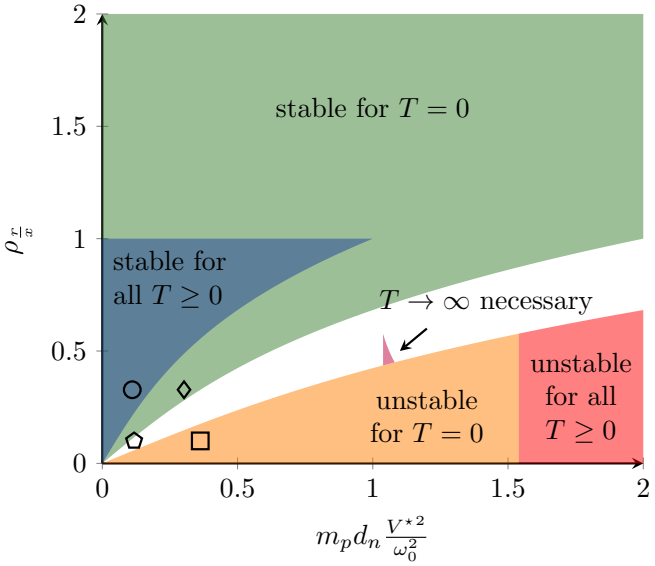

Fig. 4. Regions in the parameter space corresponding to Theorem 1 (stability), Theorem 2 (instability), and Lemma 3 (lower bound on T). Parameters for a two bus medium voltage system ($f_0 = 60$ Hz, $V^\star = 4.4$ kV, $\gamma_1 = \gamma_2 = 1$ MW, $m_p = 5\%$) with 5 km line ($\diamond$) and 5 km line including two 0.16 pu transformers ($\circ$). Parameters for a two bus high voltage system ($f_0 = 50$ Hz, $V^\star = 320$ kV, $\gamma_1 = \gamma_2 = 1$ GW, $m_p = 5\%$) with 100 km line ($\square$) and 100 km line including two 0.16 pu transformers ($\pentagon$).

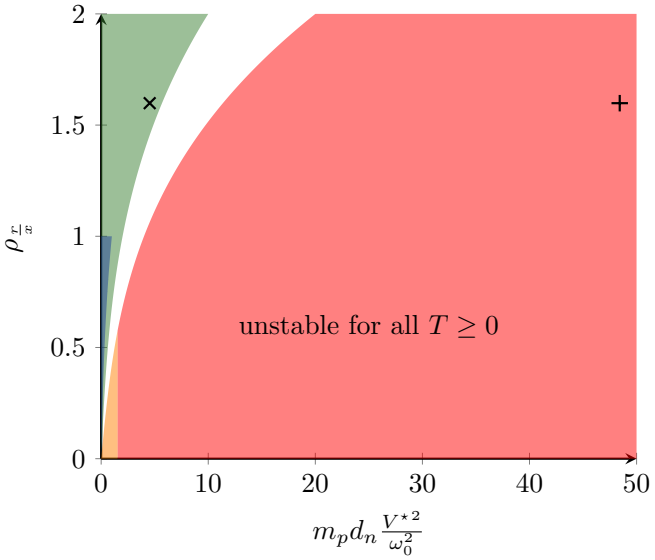

Fig. 5. Regions in the parameter space corresponding to Theorem 1 (stability) and Theorem 2 (instability). Parameters for a two bus low voltage system ($f_0 = 60$ Hz, $V^\star = 400$ V, $\gamma_1 = \gamma_2 = 20$ kW, $m_p = 1\%$) with 35 m line ($+$) and 35 m line including 0.1 pu coupling inductance ($\times$).

Lemma 3 (Lower bound on T) *Consider $g_{\omega,p}(s) = g_{\text{dr}}(s)$, $\rho_{\frac{r}{x}} \leq \sqrt{\frac{1}{3}}$, and $\lambda_N \in \mathbb{R}$ such that*

$$\frac{1}{2}\omega_0^2(\rho_{\frac{r}{x}}^{-\frac{1}{2}} + \rho_{\frac{r}{x}}^{\frac{1}{2}})^2 \geq \lambda_N m_p V^{\star 2} > 2\omega_0^2(\rho_{\frac{r}{x}} + \rho_{\frac{r}{x}}^3).$$

Then, for any stabilizing T it holds that $T > T_{\min}$ with

$$T_{\min}^2 > -\frac{r_0^2}{4\ell_0}\frac{2\omega_0^2(\rho_{\frac{r}{x}}+\rho_{\frac{r}{x}}^3)-\lambda_N m_p V^{\star 2}}{\frac{1}{2}\omega_0^2(\rho_{\frac{r}{x}}^{-\frac{1}{2}}+\rho_{\frac{r}{x}}^{\frac{1}{2}})^2-\lambda_N m_p V^{\star 2}} > 0$$

and $T_{\min} \to \infty$ as $\lambda_N m_p V^{\star 2} \to \frac{1}{2}\omega_0^2(\rho_{\frac{r}{x}}^{-\frac{1}{2}}+\rho_{\frac{r}{x}}^{\frac{1}{2}})^2$.

Proof: If $\rho_{\frac{r}{x}}^{-1} \geq \sqrt{3}$, then $2\rho_{\frac{r}{l}}(\omega_0^2+\rho_{\frac{r}{l}}^2) > \frac{1}{2\rho_{\frac{r}{l}}}(\omega_0^2+\rho_{\frac{r}{l}}^2)^2$ and under the hypothesis of the Theorem, $2\rho_{\frac{r}{l}}(\omega_0^2+\rho_{\frac{r}{l}}^2) - \lambda_N m_p V^{\star 2}\omega_0 < 0$, $\rho_{\frac{r}{l}}(\omega_0^2+\rho_{\frac{r}{l}}^2) - \lambda_N m_p V^{\star 2}\omega_0 < 0$, and $\frac{1}{2\rho_{\frac{r}{l}}}(\omega_0^2+\rho_{\frac{r}{l}}^2) - \lambda_N m_p V^{\star 2}\omega_0 \geq 0$. It directly follows that $T^2 > T_{\min}^2$ is a necessary condition for (10), i.e., necessary for asymptotic stability. ∎

Finally, the equivalence of droop control (9) and the swing equation model can be leveraged to interpret the results of this section in the context of classical multi-machine systems.

Remark 3 (Multi-machine systems) *The results of this section suggest that the use of quasi-steady-state network models in transient stability analysis of multi-machine systems is difficult to justify by the timescale separation between the network dynamics and machine rotor dynamics (i.e., large machine inertia) but can instead be justified by the large transformer and stator impedance of synchronous machines (i.e., large ℓ_{nk} resulting in small weighted node degrees d_n).*

B. Comparison with prior work

Broadly speaking, the conditions of Theorem 1 are in line with small-signal stability conditions obtained for droop control in conjunction with a reduced-order dynamic network model in [18] and the conditions for almost global stability of dVOC[3] with the line model (1) developed in [11]. However, [27] analyzes the nonlinear dVOC dynamics at operating points with non-zero power flow which naturally results in more conservative results than the small signal analysis in this work. On the other hand, the stability conditions in [18] are formulated for each pair of converters $(n,k) \in \mathcal{E}$. For brevity of the presentation we restrict our attention to small-signal frequency stability of a system of two converters. In this case, in the notation of this manuscript, the stability conditions of [18] for frequency stability for all $T \in \mathbb{R}_{\geq 0}$ reduce to

$$m_p\left(\frac{1}{\gamma_1\ell_{12}}+\frac{1}{\gamma_2\ell_{12}}\right)V^{\star 2} \leq \omega_0^2(\rho_{\frac{r}{x}}^3+2\omega_0\rho_{\frac{r}{x}}+\rho_{\frac{x}{r}}). \quad (11)$$

Moreover, $\frac{1}{\gamma_1\ell_{12}}+\frac{1}{\gamma_2\ell_{12}} = (1+\sigma_n)d_n$ for $n \in \{1,2\}$ and $\omega_0^2(\rho_{\frac{r}{x}}^3+2\omega_0\rho_{\frac{r}{x}}+\rho_{\frac{x}{r}}) > 2\omega_0^2(\rho_{\frac{r}{x}}+\rho_{\frac{r}{x}}^3)$ holds for $\rho_{\frac{r}{x}} < 1$ and $\omega_0 \geq 0$. Thus, a sufficient condition for (11) is that

$$(1+\sigma_n)d_n m_p V^{\star 2} \leq 2\omega_0^2(\rho_{\frac{r}{x}}+\rho_{\frac{r}{x}}^3) \quad (12)$$

holds for $n \in \{1,2\}$. While (12) is less conservative than Theorem 1.ii, the dynamic reduced-order model used to derive (12) typically overapproximates the stable region of the full-order model considered in this work (see [16, Fig.2]).

[3]The dVOC frequency dynamics coincide with droop control $g_{\text{dr}}(s)$ with $T = 0$ if the network is purely inductive and all voltage magnitudes are at their nominal value [27].

V. Compensation of network circuit dynamics

In this section, we show that the destabilizing effect of network circuit dynamics can be mitigated by augmenting GFM droop control with derivative droop and by leveraging derivative control terms of dual-port GFM control [21], [22].

A. Proportional-derivative droop and dual-port GFM control

We investigate a class of proportional-derivative (PD) droop control that can be used to compensate the impact of the network dynamics (1). To this end, we consider the controller

$$g_{\text{pd}}(s) = \frac{m_d s + m_p}{Ts+1}, \quad (13)$$

i.e., the VSC model (4) with $g_{\omega,p}(s) = g_{\text{pd}}(s)$ becomes

$$\theta_n(s) = -\left(\frac{1}{s}\frac{m_p+m_d s}{Ts+1}\right)\frac{p_n(s)+\delta_{p,n}(s)}{\gamma_n} + \delta_{\theta,n}(s).$$

This control is obtained by adding a realizable derivative feedback with gain $m_d \in \mathbb{R}_{>0}$ to the frequency droop control (9). Alternatively, the derivative droop term in (13) can be understood as proportional feedback from a low-pass filtered power measurement to the voltage phase angle reference [20]. While the frequency droop gain $m_p \in \mathbb{R}_{>0}$ is generally not a parameter that can be selected to ensure stability (see Remark 1), the derivative gain $m_d \in \mathbb{R}_{>0}$ is a degree of freedom that can be leveraged to ensure small-signal stability.

Moreover, droop control models the VSC as a controllable ac voltage source and neglects the dynamics of the VSC [5]. In contrast, dual-port GFM control [21], [22] explicitly leverages the VSC's dc-link dynamics modeled by

$$g_{\text{dc},n}(s) = -\frac{1}{C_{\text{dc},n}v_{\text{dc},n}^\star s + K_{\text{dc},n}} \quad (14)$$

for each VSC $n \in \mathcal{N}$. Moreover, $v_{\text{dc},n}^\star$ is the nominal dc-link voltage, $C_{\text{dc},n}$ is the dc-link capacitance, and, for brevity of the presentation, we assume that the dc source interfaced by the VSC implements a proportional dc-link voltage control with gain $K_{\text{dc},n}$ (see e.g., [21], [22] for further details). Specifically, dual-port GFM control maps the dc-link voltage $v_{\text{dc},n}$ to the VSC frequency ω_n using the controller [21], [22]

$$\omega_n(s) = \underbrace{K_{\omega,n}+K_{\theta,n}s}_{=:g_{\text{dp-gfm},n}(s)}v_{\text{dc},n}(s). \quad (15)$$

Notably, while $g_{\text{dp-gfm},n}(s)$ is not realizable, the phase angle dynamics $\theta_n = \frac{1}{s}g_{\text{dp-gfm},n}(s)v_{\text{dc},n}$ required for VSC control are realizable. The following assumption ensures that Assumption 2 holds for $g_{\text{pd}}(s) = g_{\text{dp-gfm},n}(s)g_{\text{dc},n}(s)$ and all $n \in \mathcal{N}$.

Assumption 3 (Proportionality to rating) *Given $m_p \in \mathbb{R}_{\in\mathbb{R}_{>0}}$, $T \in \mathbb{R}_{\in\mathbb{R}_{>0}}$, $m_d \in \mathbb{R}_{\geq 0}$, and the converter rating $\gamma_n \in \mathbb{R}_{\in\mathbb{R}_{>0}}$ for each bus $n \in \mathcal{N}$, it holds that $m_p = \gamma_n\frac{K_{\omega,n}}{K_{\text{dc},n}}$, $m_d = \gamma_n\frac{K_{\theta,n}}{K_{\text{dc},n}}$, and $T = \frac{C_{\text{dc},n}v_{\text{dc},n}^\star}{K_{\text{dc},n}}$.*

The next result establishes that, for any weighted node degrees d_n and any maximum local ratio of converter ratings σ_n, there exists a *large enough* derivative gain $m_d \in \mathbb{R}_{>0}$ and *small*

enough time constant $T \in \mathbb{R}_{>0}$ such that the system with PD droop control or dual-port GFM control is stable.

Theorem 3 (Stability of PD droop control) *Consider $g_{\omega,p}(s) = g_{\text{pd}}(s)$ and $m_d \in \mathbb{R}_{>0}$ such that*

$$(1+\sqrt{\sigma_n})d_n V^{\star 2}\left(\tfrac{1}{2}m_p - \omega_0 m_d \rho_{\frac{r}{x}}\right) < \omega_0^2\left(\rho_{\frac{r}{x}} + \rho_{\frac{r}{x}}^3\right)$$

for all $n \in \mathcal{N}$. Then, there exists $T_{\max} \in \mathbb{R}_{>0}$ such that $g_{\lambda_N}(s)$ is asymptotically stable for all $0 \leq T < T_{\max}$.

Proof: Using the same arguments as in the proof of Theorem 1 it follows that $g_{\lambda_N}(s)$ is asymptotically stable if and only if

$$\begin{aligned} 4\rho_{\frac{r}{l}}^2 \left(\left(\frac{\omega_0^2+\rho_{\frac{r}{l}}^2+\xi_d}{2\rho_{\frac{r}{l}}} - \frac{\xi_d}{4\rho_{\frac{r}{l}}^2}\right)(\omega_0^2+\rho_{\frac{r}{l}}^2+\xi_d) - \xi_p\right) T^2 \\ +4\rho_{\frac{r}{l}}\left(\rho_{\frac{r}{l}}(\omega_0^2+\rho_{\frac{r}{l}}^2+\xi_d) - \xi_p\right) T \\ +2\rho_{\frac{r}{l}}(\omega_0^2+\rho_{\frac{r}{l}}^2+\xi_d) - \xi_p > 0 \end{aligned}$$

holds for $\xi_p = \lambda_N m_p V^{\star 2}\omega_0$ and $\xi_d = \lambda_N m_d V^{\star 2}\omega_0$. By Lemma 2, the hypothesis of the Theorem implies that $2\rho_{\frac{r}{l}}(\omega_0^2+\rho_{\frac{r}{l}}^2+\xi_d) > \xi_p$ and the Theorem directly follows. ■

This result significantly improves upon Theorem 1. In particular, in practice, the time constant $T \in \mathbb{R}_{>0}$ of droop control with low-pass filter is often small and used to filter switching harmonics. Likewise, the time constant $T \in \mathbb{R}_{>0}$ of dual-port GFM control is proportional to the size of the dc-link capacitor (see Assumption 3) that is typically small. Thus, while Theorem 3 does not provide any explicit bounds on $T \in \mathbb{R}_{>0}$, the conditions of Theorem 3 are realistic in the sense that they show that stability can be achieved for small time constants $T \in \mathbb{R}_{>0}$ as opposed to very large time constants $T \in \mathbb{R}_{>0}$ for standard droop control (see e.g., Lemma 3). Obtaining explicit bounds that related $m_d \in \mathbb{R}_{>0}$, $T \in \mathbb{R}_{>0}$, d_n, and σ_n is seen as an interesting topic for future work.

The following corollary directly follows from Theorem 3 and Lemma 2, and highlights that for $m_d \geq \frac{m_p}{2\omega_0}\rho_{\frac{r}{x}}^{-1}$ and $T = 0$, the system is stable independently of the weighted node degrees d_n and maximum local ratio of converter ratings σ_n.

Corollary 1 (Stability for any network) *Consider $g_{\omega,p}(s) = g_{\text{pd}}(s)$ with $T = 0$ and $m_d \geq \frac{m_p}{2\omega_0}\rho_{\frac{r}{x}}^{-1}$. Then, $g_{\lambda_N}(s)$ is asymptotically stable.*

This result shows that PD droop (13) control with $T = 0$ significantly improves upon the stability region of regular droop control (9) (both with (i.e., $T \in \mathbb{R}_{>0}$) and without (i.e. $T = 0$) inertia emulation). However, for systems with small resistance-reactance ratio $\rho_{\frac{r}{x}}$, using $m_d = \frac{m_p}{2\omega_0}\rho_{\frac{r}{x}}^{-1}$ may result in prohibitively large derivative gains m_d. Generally, stability can typically be guaranteed for such systems without derivative gain (see Theorem 1). However, one may envision systems, such as transmission connected plants containing many devices with low power rating connected through short lines, for which Theorem 1 cannot be used to certify stability and Corollary 1 results in prohibitively large gains m_d. Investigating such scenarios is seen as an interesting topic for future research.

B. Frequency and angle droop

Finally, we consider the frequency and angle droop control

$$g_{\text{fa}}(s) = \frac{m_p}{Ts+1} + m_d s, \tag{16}$$

that results in the voltage phase angle dynamics

$$\theta_n(s) = -\left(\frac{1}{s}\frac{m_p}{Ts+1} + m_d\right)\frac{p_n(s)+\delta_{p,n}(s)}{\gamma_n} + \delta_{\theta,n}(s).$$

In other words, a direct feedback from active power to voltage phase angle without low-pass filter is used. For this control, the derivative gain $m_d \in \mathbb{R}_{>0}$ is again a degree of freedom that can be leveraged to ensure small-signal stability while the frequency droop gain m_p is typically prescribed by system-level objectives (see Remark 1).

Remark 4 (Virtual impedance) *The transfer function* (16) *also arises as the linearization of standard droop control* (9) *in combination with a purely inductive virtual impedance [28]. We note that virtual impedance does not emulate the dynamics* (1) *of an impedance but only its steady-state response. Moreover, virtual impedance inevitably impacts the steady-state voltage magnitude and frequency. In contrast,* (16) *compensates network dynamics without impact on the steady-state of the power system.*

The next result shows that for any $T \in \mathbb{R}_{\geq 0}$, $m_p \in \mathbb{R}_{>0}$, $\lambda_N \in \mathbb{R}_{>0}$, and $\rho_{\frac{r}{x}} \in \mathbb{R}_{>0}$, there always exists a *large enough* derivative gain $m_d \in \mathbb{R}_{>0}$ such that the power system is stable. Moreover, if the reactance-resistance ratio $\rho_{\frac{r}{x}}$ is sufficiently small (i.e., in high voltage or medium voltage systems), then there exists a derivative gain $m_d \in \mathbb{R}_{>0}$ that renders the power system stable for all $T \in \mathbb{R}_{\geq 0}$.

Theorem 4 (Stability of frequency and angle droop control) *Consider $g_{\omega,p}(s) = g_{\text{fa}}(s)$. Then, for any $T \in \mathbb{R}_{\geq 0}$ there exists $m_d \in \mathbb{R}_{>0}$ such that $g_{\lambda_N}(s)$ is asymptotically stable. Moreover, if $\rho_{\frac{r}{x}} < 1$, then $g_{\lambda_N}(s)$ is asymptotically stable for all $T \in \mathbb{R}_{\geq 0}$ if, for all $n \in \mathcal{N}$, it holds that*

$$(1+\sqrt{\sigma_n})d_n V^{\star 2}\left(m_p - \omega_0 m_d \rho_{\frac{r}{x}}\right) < \omega_0^2\left(\rho_{\frac{r}{x}} + \rho_{\frac{r}{x}}^3\right).$$

Proof: Using the same arguments as in the proof of Theorem 1, $\xi_p = \lambda_N m_p V^{\star 2}\omega_0$, and $\xi_d = \lambda_N m_d V^{\star 2}\omega_0$, it follows that $g_{\lambda_N}(s)$ is asymptotically stable if and only if

$$\begin{aligned} 4\rho_{\frac{r}{l}}^2\left(\frac{1}{2}\rho_{\frac{r}{l}}^{-1}(\omega_0^2+\rho_{\frac{r}{l}}^2+\xi_d)^2 - \xi_p\right)T^2 + \\ 4\rho_{\frac{r}{l}}\left(\rho_{\frac{r}{l}}(\omega_0^2+\rho_{\frac{r}{l}}^2+\xi_d) - \xi_p\right)T + \\ 2\rho_{\frac{r}{l}}(\omega_0^2+\rho_{\frac{r}{l}}^2+\xi_d) - \xi_p > 0. \end{aligned} \tag{17}$$

It directly follows that one can always find a large enough $m_d \in \mathbb{R}_{>0}$ such that (17) holds for any $T \in \mathbb{R}_{>0}$. Moreover, if $\rho_{\frac{r}{x}} < 1$, then, under the hypothesis of the Theorem, $\frac{1}{2}\rho_{\frac{r}{l}}^{-1}(\omega_0^2+\rho_{\frac{r}{l}}^2+\xi_d)^2 - \xi_p > \rho_{\frac{r}{l}}(\omega_0^2+\rho_{\frac{r}{l}}^2+\xi_d) - \xi_p > 0$ for all ξ_p. Next, considering Lemma 2, the Theorem follows because $\rho_{\frac{r}{l}}(\omega_0^2+\rho_{\frac{r}{l}}^2+\xi_d) > \xi_p$ under the hypothesis of the Theorem. ■

The following simplified stability condition is a direct consequence of Theorem 4.

Corollary 2 (Stability for any network with $\rho_{\frac{r}{x}} < 1$) *Consider $g_{\omega,p}(s) = g_{\text{fa}}(s)$ and $m_d > \frac{m_p}{\omega_0}\rho_{\frac{r}{x}}^{-1}$. Then, $g_{\lambda_N}(s)$ is asymptotically stable for all $T \in \mathbb{R}_{\geq 0}$ and any network with $\rho_{\frac{r}{x}} < 1$.*

Similarly to Corollary 1 for droop control with $T = 0$, selecting m_d based on Corollary 2 may result in prohibitively large derivative control gains in systems with small resistance-reactance ratios $\rho_{\frac{r}{x}}$. The reader is referred to the discussion below Corollary 1 for further details.

VI. Conclusion

This work analyzed the impact of network circuit dynamics on grid-forming control and highlighted that the network circuit dynamics cannot be neglected in transient stability analysis of converter-dominated power systems. Contrary to conventional wisdom, the analytic stability conditions developed in this work show that instability induced by network circuit dynamics cannot always be avoided by slowing down the voltage phase angle dynamics of grid-forming converters or may require unrealistic virtual inertia constants. Moreover, this work proposed to augment grid-forming droop control with derivative feedback to compensate the network dynamics and provides analytical stability conditions for proportional-derivative droop control and dual-port grid-forming control that account for network circuit dynamics. The results indicate that derivative droop terms are a promising solution to compensate network circuit dynamics in grid-forming control.

References

[1] F. Milano, F. Dörfler, G. Hug, D. J. Hill, and G. Verbič, "Foundations and challenges of low-inertia systems (invited paper)," in *Power Systems Computation Conference*, 2018.

[2] D. Dong, B. Wen, D. Boroyevich, P. Mattavelli, and Y. Xue, "Analysis of phase-locked loop low-frequency stability in three-phase grid-connected power converters considering impedance interactions," *IEEE Trans. Ind. Electron.*, vol. 62, no. 1, pp. 310–321, 2015.

[3] "1200 MW fault induced solar photovoltaic resource interruption disturbance report," NERC, Tech. Rep., 2017.

[4] J. Matevosyan, B. Badrzadeh, T. Prevost, E. Quitmann, D. Ramasubramanian, H. Urdal, S. Achilles, J. MacDowell, S. H. Huang, V. Vital, J. O'Sullivan, and R. Quint, "Grid-forming inverters: Are they the key for high renewable penetration?" *IEEE Power Energy Mag.*, vol. 17, no. 6, pp. 89–98, 2019.

[5] A. Tayyebi, D. Groß, A. Anta, F. Kupzog, and F. Dörfler, "Frequency stability of synchronous machines and grid-forming power converters," *IEEE Trans. Emerg. Sel. Topics Power Electron.*, vol. 8, no. 2, pp. 1004–1018, 2020.

[6] M. Chandorkar, D. Divan, and R. Adapa, "Control of parallel connected inverters in standalone ac supply systems," *IEEE Trans. Ind. Appl.*, vol. 29, no. 1, pp. 136–143, 1993.

[7] J. Rocabert, A. Luna, F. Blaabjerg, and P. Rodríguez, "Control of power converters in ac microgrids," *IEEE Trans. Power Electron.*, vol. 27, no. 11, pp. 4734–4749, 2012.

[8] S. D'Arco, J. A. Suul, and O. B. Fosso, "A virtual synchronous machine implementation for distributed control of power converters in smartgrids," *Electr. Pow. Sys. Res.*, vol. 122, pp. 180–197, 2015.

[9] L. Tôrres, J. Hespanha, and J. Moehlis, "Synchronization of identical oscillators coupled through a symmetric network with dynamics: A constructive approach with applications to parallel operation of inverters," *IEEE Trans. Autom. Control*, vol. 60, no. 12, pp. 3226–3241, 2015.

[10] B. Johnson, S. Dhople, A. Hamadeh, and P. Krein, "Synchronization of parallel single-phase inverters with virtual oscillator control," *IEEE Trans. Power Electron.*, vol. 29, no. 11, pp. 6124–6138, 2014.

[11] D. Groß, M. Colombino, B. Jean-Sébastien, and F. Dörfler, "The effect of transmission-line dynamics on grid-forming dispatchable virtual oscillator control," *IEEE Trans. Control Netw. Syst.*, vol. 6, no. 3, pp. 1148–1160, 2019.

[12] B. K. Poolla, D. Groß, and F. Dörfler, "Placement and implementation of grid-forming and grid-following virtual inertia and fast frequency response," *IEEE Trans. Power Syst.*, vol. 34, no. 4, pp. 3035–3046, 2019.

[13] R. H. Lasseter, Z. Chen, and D. Pattabiraman, "Grid-forming inverters: A critical asset for the power grid," *IEEE Trans. Emerg. Sel. Topics Power Electron.*, vol. 8, no. 2, pp. 925–935, 2020.

[14] A. Crivellaro, A. Tayyebi, C. Gavriluta, D. Groß, A. Anta, F. Kupzog, and F. Dörfler, "Beyond low-inertia systems: Massive integration of grid-forming power converters in transmission grids," in *IEEE Power & Energy Society General Meeting*, 2020.

[15] V. Mariani, F. Vasca, J. C. Vásquez, and J. M. Guerrero, "Model order reductions for stability analysis of islanded microgrids with droop control," *IEEE Trans. Ind. Electron.*, vol. 62, no. 7, pp. 4344–4354, 2015.

[16] P. Vorobev, P.-H. Huang, M. Al Hosani, J. L. Kirtley, and K. Turitsyn, "High-fidelity model order reduction for microgrids stability assessment," *IEEE Trans. Power Syst.*, vol. 33, no. 1, pp. 874–887, 2018.

[17] U. Markovic, O. Stanojev, P. Aristidou, E. Vrettos, D. Callaway, and G. Hug, "Understanding small-signal stability of low-inertia systems," *IEEE Trans. Power Syst.*, vol. 36, no. 5, pp. 3997–4017, 2021.

[18] P. Vorobev, P.-H. Huang, M. Al Hosani, J. L. Kirtley, and K. Turitsyn, "A framework for development of universal rules for microgrids stability and control," in *IEEE Conf. on Dec. and Contr.*, 2017, pp. 5125–5130.

[19] I. Subotić, D. Groß, M. Colombino, and F. Dörfler, "A lyapunov framework for nested dynamical systems on multiple time scales with application to converter-based power systems," *IEEE Trans. Autom. Control*, vol. 66, no. 12, pp. 5909–5924, 2021.

[20] A. Engler, "Device for parallel operation of equal range single-phase or three-phase voltage sources," Patent EP1 286 444B1, 2001.

[21] D. Groß, E. Sánchez-Sánchez, E. Prieto-Araujo, and O. Gomis-Bellmunt, "Dual-port grid-forming control of mmcs and its applications to grids of grids," *IEEE Trans. Power Del.*, 2022.

[22] X. Lyu, I. Subotić, and D. Groß, "Unified grid-forming control of pmsg wind turbines for fast frequency response and MPPT," in *IREP Bulk Power System Dynamics and Control Symposium*, 2022.

[23] P. W. Sauer and M. A. Pai, *Power System Dynamics and Stability*. Prentice Hall, 1998.

[24] F. Paganini and E. Mallada, "Global analysis of synchronization performance for power systems: Bridging the theory-practice gap," *IEEE Trans. Autom. Control*, vol. 65, no. 7, pp. 3007–3022, 2020.

[25] B. Brogliato, B. Maschke, R. Lozano, and O. Egeland, *Positive Real Systems*. Springer, 2007, pp. 9–68.

[26] J. Schiffer, D. Goldin, J. Raisch, and T. Sezi, "Synchronization of droop-controlled microgrids with distributed rotational and electronic generation," in *IEEE Conf. on Dec. and Contr.*, 2013, pp. 2334–2339.

[27] G.-S. Seo, M. Colombino, I. Subotiċ, B. Johnson, D. Groß, and F. Dörfler, "Dispatchable virtual oscillator control for decentralized inverter-dominated power systems: Analysis and experiments," in *IEEE Applied Power Electron. Conf. and Exposition*, 2019, pp. 561–566.

[28] J. He and Y. W. Li, "Analysis, design, and implementation of virtual impedance for power electronics interfaced distributed generation," *IEEE Trans. Ind. Appl.*, vol. 47, no. 6, pp. 2525–2538, 2011.